Advantages of Infinite Elements over Pre-specified Boundary Conditions in Unbounded Problems

Dr. Aykut Erkal, Assistant Professor,
School of Engineering & Architecture, Department of Civil Engineering,
İstanbul Kemerburgaz University
Mahmutbey Dilmenler Caddesi, No: 26, 34217 Bağcılar, İstanbul, TURKEY;
Phone: +90-212-604 01 00 (extension: 1407); Mobile: +90-532-470 84 12;
Fax: + 90-212-445 92 55;
E-mail: erkala@hotmail.com

Corresponding Author
Dr. Debra F. Laefer, Associate Professor
School of Civil, Structural & Environmental Engineering,
University College Dublin (UCD), Dublin 4, Ireland;
Phone: +353-1-716-3226; Fax: +353-1-716-3297;
E-mail: debra.laefer@ucd.ie

Dr. Semih Tezcan, Professor
Faculty of Engineering, Department of Civil Engineering,
Boğaziçi University, Bebek, İstanbul, 34342, Turkiye;
Phone: +90-212-352 65 59, Mobile: +90-532-371 03 40, Fax: +90-212-352 65 58
E-mail: Tezokan@superonline.com

ABSTRACT

This paper promotes the further development and adoption of infinite elements for unbounded problems. This is done by demonstrating the ease of application and computational efficiency of infinite elements. Specifically, this paper introduces a comprehensive set of coordinate and field variable mapping functions of one-dimensional and two-dimensional infinite elements, not previously available. Performance is then benchmarked against various parametric models for deflection and stress in two cases: (1) a circular, uniformly-distributed load and (2) a point load on a semi-infinite, axi-symmetrical medium. The results of each case are compared with its closed-form solution. As an example, when the vertical deflections in example 2 are compared to the closed form solution, the 45% error level generated with fixed boundaries and 14% generated with spring-supported boundaries is reduced to only 1% with infinite elements, even with a coarse mesh. Perceptions about the complexity in using infinite elements and the prior absence of comprehensive comparisons of equivalent meshes may account for the slow rate of adoption of this powerful approach.

Key Words: infinite elements, unbounded problem, far field domain, finite element method, Boussinesq problem

INTRODUCTION

In several fields of engineering and science, many problems have domains that are assumed to extend to infinity, such as soil-structure interaction (Kazakov 2010), seepage (Zhao and Valliappan 1993), sediment transport and fluid flow (Xia and Zhang 2006), wave propagation (Yang et al. 2003), and thermal transient problems (Damjanlc' 1984). Examples include waves behind a breakwater, an airplane wing moving through air, a dam supported by the ground, and an aerofoil in flowing water (Fig. 1). For such problems, analysis extends to large distances in one or more directions to represent the far field domain (unbounded domain). The major difficulty for the numerical solution of these problems is the discretization of the unbounded domain.

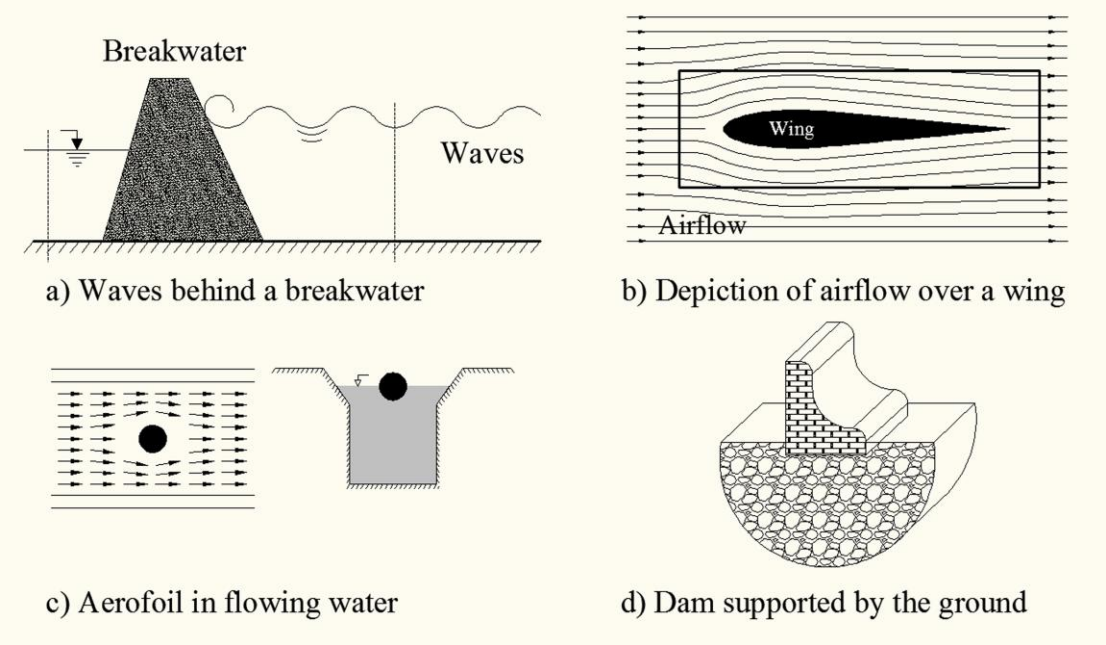

Figure 1. Application areas of infinite elements

One solution is to truncate the domain of analysis at large, finite distances from the load application location, to a point where the applied load influence is deemed small enough to be neglected (i.e. use of an artificial boundary) and to apply appropriate boundary conditions (i.e. fixed or movable displacement, constant stress, viscous, absorbing, or transmitting) as described extensively by Deeks and Randolph (1994). This approach generally requires experimentation with grid sizes and boundary conditions. Additionally, the analysis approach may require validation through simpler problems with analytical solutions, if available. A further

disadvantage to this approach is that an extensive number of node points may be involved strictly in modeling the remote region, where the perturbation in the stress or displacement field is virtually zero. Furthermore, in dynamic analyses, an artificial boundary can lead to considerable errors due to the reflection of the propagating waves (Kausel 1988). For static problems, simple truncation at a rigid boundary may work satisfactorily; however, truncation location selection is non-exact, and computational compromise is necessary. Namely, the further the truncation boundary is placed from the area of interest, the better the accuracy but the higher the computational expense.

To overcome these limitations, various modeling approaches have been developed such as the boundary elements method (Katsikadelis 2002), the system identification approach, and the introduction of viscous or transmitting boundaries in the modeling (Deeks and Randolph 1994). Alternatively, infinite elements are similar to the finite elements, except in the infinite direction. Specifically, they have one or more dimensions of infinite extent in physical space. Informally, nodes of such elements are described as "going to infinity". The other advantage is that edge compatibility between finite and infinite elements based on the continuity of deformations of adjoining nodes is satisfied in an identical manner as between finite elements.

To achieve this, the near field domain is discretized with the finite elements, depending on the required sensitivity, while the far field domain is discretized by the infinite elements only along the boundary, thus rendering an economical modeling of the unbounded domain. Various forms of field shape functions are introduced over infinite elements, which then decay to zero at infinity. Several types of shape functions (which extend to infinity) are utilized to generate infinite elements (Bettess 1992).

Despite the novelty and effectiveness of this approach, infinite element adoption has been slow. Arguably this is in part due to the perceived complexity of the approach and the absence of easily understood comparison of equivalent meshes. To help overcome these obstacles, the remainder of this paper is as follows. First the history, development, and application of infinite elements are provided. Next, the derivation of matrix properties of infinite elements is shown with a comprehensive set of coordinate and field variable mapping functions of one-dimensional (1-D) and two-dimensional (2-D) infinite elements. Finally, numerical examples are furnished to

illustrate the advantages and disadvantages of modeling strategies of unbounded domain problems.

ORIGINS AND DEVELOPMENT OF INFINITE ELEMENTS

In 1973, Ungless and Anderson introduced and named the first infinite element Ungless 1973, Anderson and Ungless 1977). They employed a simple shape function, which varied as $1/(1+r)$ in the radial direction. The three-dimensional (3-D), infinite element has a triangular base (defined as being perpendicular in the local *xy*-plane) and extends from this base to infinity. This triangular prism-shaped element has the z-direction defined as perpendicular to the base and as being infinite (Fig. 2a). Unfortunately, as also noted by Ungless (1973), this can cause incompatibilities between adjacent elements, if the bases of adjacent elements are not parallel. Analytical integration in the *xy*-plane and numerical integration in the *z*-direction is utilized to form the element matrices. The closed form solution of a Boussinesq point load on a semi-infinite medium was used to validate the effectiveness of the element (Fig. 2b).

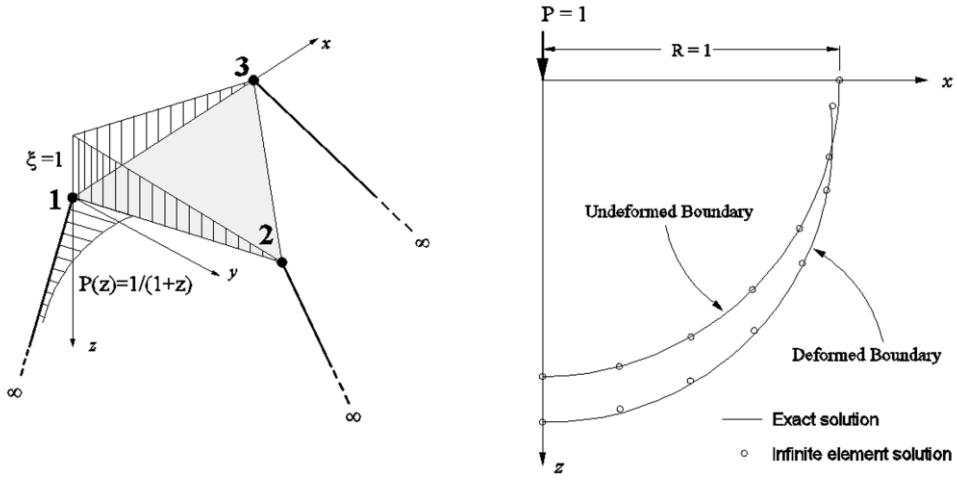

Figure 2. Infinite Element by Ungless and Anderson (1973)

Zienkiewicz and Bettess (1975) subsequently utilized infinite elements for fluid structure interaction problems. The element domain was extended to infinity, employing an original finite

element as its basis. The field variable shape function was multiplied by an appropriate decay function to obtain the desired behavior at infinity, for a particular problem (Fig. 3). The first decay functions used by Bettess was composed of a polynomial multiplied by an exponential term with a negative power *(exp (-r))*, and infinite element matrices were formed using analytical integrations. The approach was first applied to simple one-dimensional (1-D) examples (Bettess 1977), and then to more complicated two-dimensional (2-D) and axi-symmetric problems (Bettess 1980, Bettess and Zienkiewicz 1977).

Ultimately, mapping techniques were used to form infinite elements. For instance, Medina (1981) used Anderson and Ungless's mapping technique (1977) to solve Boussinesq and Cerutti problems. Also, Medina (1980) contrived an axi-symmetric infinite element to solve three-dimensional (3-D) wave propagation problems in cylindrical, orthotropic, elastic, unbounded continua. In the frequency domain, Rayleigh, shear and compression wave propagation were modeled with this element. However, the first explicit mapping was developed by Beer and Meek (1981), who used a shape function to map a finite domain onto an infinite domain, thereby splitting the mapping into two parts for finite and infinite directions. Zienkiewicz et. al. (1983) also proposed a not dissimilar infinite element with a simpler mapping solution methodology and convergence advantages. The mapping was used for both the geometry transformation and unknown function transformation from the local to the global coordinate system; higher orders of shape function ensured better convergence (Zienkiewicz et al. 1983).

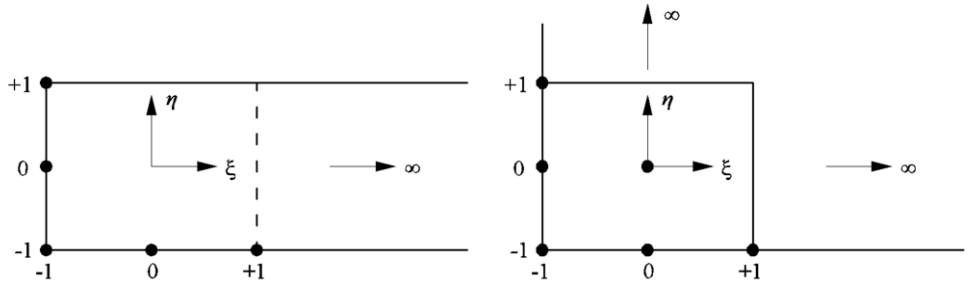

Figure 3. Geometry of typical decay function of infinite elements (Bettess 1980)

Later, Simoni and Schrefler (1987) applied mapped infinite elements in a pair of consolidation problems. Subsequently, Zhao and Valliappan (1993) presented a time-dependent infinite

element to simulate transient seepage problems in infinite media. In order to examine the accuracy and efficiency of the infinite elements, they solved both a 1-D transient seepage problem in a semi-infinite medium and a 2-D transient seepage problem in a full plane using the finite and infinite elements.

ELEMENT CLASSIFICATIONS

Infinite elements can be categorized according to their geometrical configurations, type of analysis, and their formulation. Due to the idealization needs in the solution process of each problem, the model can be 1-D, 2-D, or 3-D to decrease computational expense and, thus, solution time [Abdel-Fattah et al. 2000]. Depending on the nature of the analysis, infinite elements can also be grouped into static and dynamic types (Khalili et al. 1997).

The most common classification is, however, made according to the field variable mapping and the coordinate mapping. They are called decay function infinite elements (also known as displacement descent elements) or mapped infinite elements (also known as coordinate ascent elements). To develop decay function infinite elements, the field variable shape function of an infinite element is multiplied by a decay function, which causes the field variable to approach the value at infinity. The conventional finite element shape functions are inappropriate to describe the behavior of the field variables at infinity. Thus, decay functions are introduced (Koh and Lee 1998) to modify the finite element shape functions resulting in the behavior of the element to be a reasonable reflection of the problem at infinity. Decay functions can be exponential, reciprocal, or logarithmic. Mapped infinite elements are the other type. Conventional shape functions are used to describe the variation of the field variable, while the geometry is mapped from a finite to an infinite domain using growth shape functions in the infinite direction (Zienkiewicz et al. 1983). The growth shape function grows without bounds, as the natural coordinate approaches a particular value. This presents theoretical advantages and formulation simplicity for the mapped infinite elements. Additionally, the degree of the decay of a field variable is not imposed with a specific decay function, which precludes predetermining the solution of a problem.

THEORETICAL DERIVATIONS

In the process of developing the stiffness properties of mapped infinite elements, the conventional finite elements are modified to contain some nodes and element boundaries, which model the domain stretching to infinity. The derivation of the stiffness matrix of a three-node, 1-

D, infinite element is presented. Additionally, the shape functions of an eight-node, 2-D, mapped infinite element are illustrated in detail.

A One-dimensional Three-node Mapped Infinite Element

Details of the one-dimensional three-node mapped infinite element are presented in Fig. 4. The distance *a* between nodes 1 and 2 is considered a characteristic length of the element. Figure 4 also shows a point labeled 0, at a distance *a* from point 1. This point is not a node but a pole.

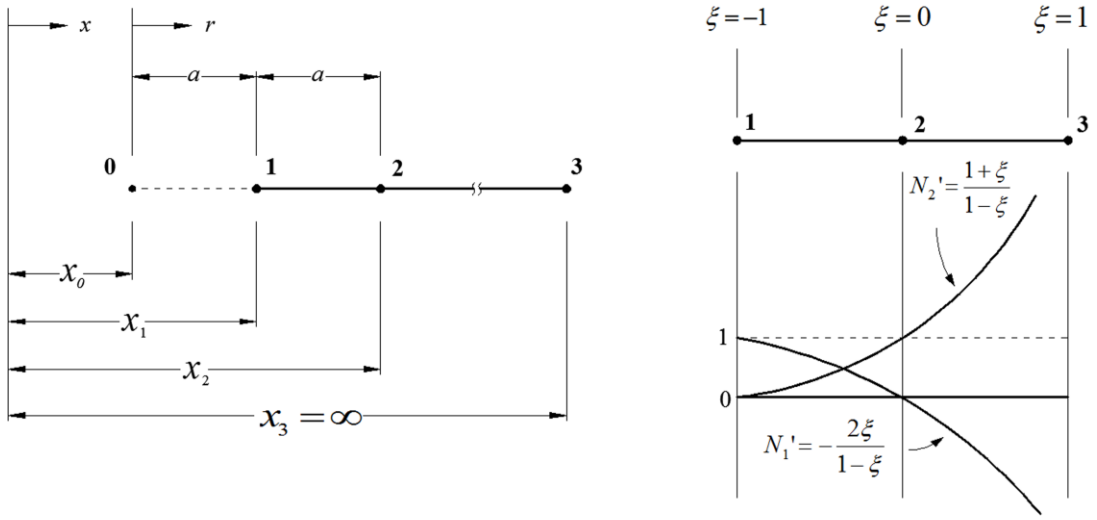

a) Physical Space b) Natural Coordinate Space

Figure 4. A one-dimensional, three-node mapped infinite element

Geometry Interpolation

The element geometry is interpolated according to two mapping functions (growth shape functions), N_1 and N_2, which are rational in the natural coordinate ξ:

$$\{x\} = \{N_1 \quad N_2\} \begin{Bmatrix} x_1 \\ x_2 \end{Bmatrix} \qquad (1)$$

in which,

$$N_1 = -\frac{2\xi}{1-\xi}, \qquad N_2 = \frac{1+\xi}{1-\xi}. \qquad (2)$$

Notably $x = x_1$ and $x = x_2$ for $\xi = -1$ and $\xi = 0$, respectively. However, $x \to \infty$, for $\xi = 1$. Thus, the mapping in Equation (1) automatically places node 3 at infinity, and the geometric interpolant need not explicitly contain node 3, as seen in equation (3).

$$x_3 = \lim_{\xi \to 1} \frac{-2\xi x_1 + (1+\xi)x_2}{1-\xi} = \infty \qquad (3)$$

Field Variable Interpolation

A generic field variable is interpolated over the infinite element by the standard shape functions of the 3-node line element

$$\{u\} = \{L_1 \quad L_2 \quad L_3\} \begin{Bmatrix} d_1 \\ d_2 \\ d_3 \end{Bmatrix} \quad (4)$$

where,

$$L_1 = -\frac{1}{2}\xi(1-\xi), \quad L_2 = 1-\xi^2, \quad L_3 = \frac{1}{2}\xi(1+\xi) \quad (5)$$

They are written in accordance with Lagrangian Shape Functions in Equation 6 for the 3-node line element, as shown in Figure 5.

$$N(x) = \prod_{\substack{j=1 \\ (i \neq j)}}^{j=n} \frac{(\xi - \xi_j)}{(\xi_i - \xi_j)} \qquad (6)$$

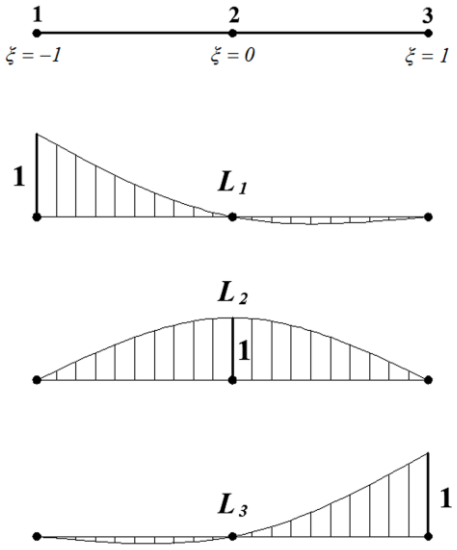

Figure 5. Shape functions of three-node line element for field variables

To show the representation of u in terms of the physical coordinates x, ξ can be solved from the geometric interpolant. Equation (1) is rewritten as equation (7).

$$\{x\} = \begin{Bmatrix} -\dfrac{2\xi}{1-\xi} & \dfrac{1+\xi}{1-\xi} \end{Bmatrix} \begin{Bmatrix} x_1 \\ x_2 \end{Bmatrix} \qquad (7)$$

If equation (7) is solved for ξ, and the relationships $x_1 = x_0 + a$, $x_2 = x_0 + 2a$ and $r = x - x_0$ are substituted, Equation (8) results.

$$\xi = \frac{x - x_2}{x + x_2 - 2x_1} = 1 - \frac{2a}{r} \qquad (8)$$

The variation of $\{u\}$ by ξ can be written by the help of equations (4) and (5) as:

$$\{u\} = \begin{Bmatrix} -\frac{1}{2}\xi(1-\xi) & (1-\xi^2) & \frac{1}{2}\xi(1+\xi) \end{Bmatrix} \begin{Bmatrix} d_1 \\ d_2 \\ d_3 \end{Bmatrix} (9)$$

If Equation (8) is substituted into Equation (9), then Equation (10) is obtained.

$$u = d_3 + (-d_1 + 4d_2 - 3d_3)\frac{a}{r} + 2(d_1 - 2d_2 + d_3)\frac{a^2}{r^2} \quad (10)$$

As $r \to \infty$, $u \to d_3$, which is set to zero ($d_3 = 0$) as a boundary condition. If $d_1 = d_2 = d_3 = C$, then the constant value $u = C$ represents rigid body movement. In general, the two parenthetical expressions in equation (10) do not vanish, so *u* becomes infinite at point 0, because *r = 0* at point *0*. Point *0* is, therefore, a pole or singular point about which the field quantity *u* decays. The presence of the decay functions is noted ($1/r$, $1/r^2$). The coefficients of these terms are generally not zero. Also, as $r \to a$, $u \to d_1$ and $r \to 2a$, then $u \to d_2$, as expected ($d_3 = 0$ for static analysis). The strain component can be obtained by differentiating equation (10), with respect to *x*:

$$\frac{du}{dx} = \frac{du}{dr}\frac{dr}{dx} = \left(d_1 - 4d_2 + 3d_3\right)\frac{a}{r^2} - 4\left(d_1 - 2d_2 + d_3\right)\frac{a}{r^3} \qquad (11)$$

in which $\frac{dr}{dx} = 1$. In the matrix form, the strain vector is obtained as the *x* derivative of *u* as follows:

$$\{\varepsilon_x\} = [\Delta]\{u\} = [\Delta]\{L\}\{d\} = [G]\{d\} = J^{-1}\left\{\left(-1/2 + \xi\right) \quad \left(-2\xi\right) \quad \left(1/2 + \xi\right)\right\} \begin{Bmatrix} d_1 \\ d_2 \\ d_3 \end{Bmatrix} \qquad (12)$$

where $[\Delta]$ is the operator matrix to differentiate the field variable shape function matrix $[L]$. The generic and nodal displacements are $\{u\}$ and $\{d\}$, respectively. The strain matrix is $[G]$ and J^{-1} is the inverse of Jacobian matrix. The stiffness matrix of the 1-D infinite element can be obtained by the usual expression:

$$[K] = \int_V [G]^T [D][G]\, dV \qquad (13)$$

where $[G] = \frac{\left(1-\xi^2\right)}{2a}\left\{\left(-1/2 + \xi\right) \quad \left(-2\xi\right) \quad \left(1/2 + \xi\right)\right\}$, material matrix $[D] = E$, and $dV = Adx = AJd\xi$.

Thus,

$$[K] = \int_{-1}^{+1} EA[G]^T [G] J d\xi \tag{14}$$

and

$$[K] = EA \int_{-1}^{+1} \frac{\left(1-\xi^2\right)}{2a} \begin{Bmatrix} \left(-1/2+\xi\right) \\ \left(-2\xi\right) \\ \left(1/2+\xi\right) \end{Bmatrix} \frac{\left(1-\xi^2\right)}{2a} \left\{ \left(-1/2+\xi\right) \quad \left(-2\xi\right) \quad \left(1/2+\xi\right) \right\} J d\xi \tag{15}$$

After the integration, the stiffness matrix of an infinite 1-D element (Figure 4a) is obtained as Equation (16)

$$[K] = \frac{EA}{2a} \begin{bmatrix} 46/15 & -52/15 & 2/5 \\ -52/15 & 64/15 & -4/5 \\ 2/5 & -4/5 & 2/5 \end{bmatrix} \tag{16}$$

which can be used in the master stiffness matrix of the global system. The above derivation of the mapping functions were for 1-D infinite elements, extending to infinity in one direction. A similar approach can be adopted for 2-D and 3-D infinite elements.

Two-dimensional Mapped Infinite Element

Geometrical configuration, coordinate mapping, and field variable mapping functions of two-dimensional infinite elements used in example 2 are discussed here. Keeping the idea of a mapped function approach in mind, extending the formulation to 2-D infinite elements is straightforward. For those elements, growth shape functions are used in the infinite direction, and standard shape functions are applied in the finite direction.

Coordinate mapping can be performed through the product of a growth function $\left(G_j\right)$ in the infinite direction and a Lagrangian function; $\left(L_k\right)$ in the finite direction [Equation (17)] for the element with a single infinite direction. Subscripts j and k denotes natural coordinates ξ and η.

$$\{x\} = \left(G_j\right)\left(L_k\right)\{x_i\} \tag{17}$$

For the element with two-infinite directions, however, growth functions are used for both of the directions [Equation (18)].

$$\{x\} = \left(G_j\right)\left(G_k\right)\{x_i\} \tag{18}$$

Figure 6 shows geometrical configurations of 2-D, mapped infinite elements in 1- and 2-infinite directions. Their shape functions are given in Table 1.

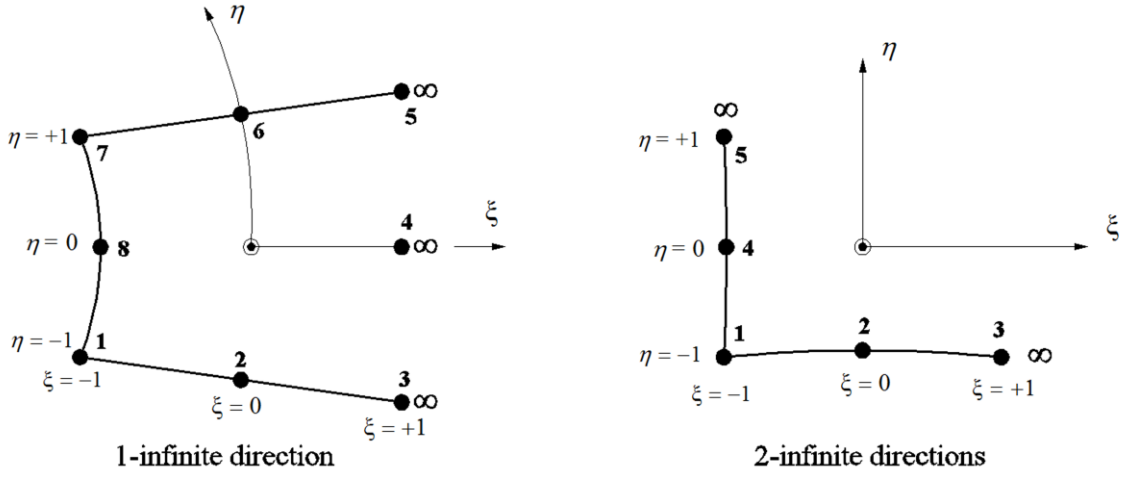

Figure 6. Geometrical configuration of 2-D, mapped infinite element

Table 1. Shape functions for 2-D infinite elements

1-infinite direction	Node Numbers	Shape Functions	2-infinite direction	Node Numbers	Shape Functions
	1 and 7	$\frac{\left(-1-\xi-\xi\eta\eta_i+\eta^2\right)}{\left(1-\xi\right)}$		1	$\frac{-4\left(1+\xi+\eta\right)}{\left(1-\xi\right)\left(1-\eta\right)}$
	2 and 6	$\frac{\left(1+\xi\right)\left(1+\eta\eta_i\right)}{2\left(1-\xi\right)}$		2	$\left(\frac{1+\xi}{1-\xi}\right)\left(\frac{2}{1-\eta}\right)$
	8	$\frac{2\left(1-\eta^2\right)}{\left(1-\xi\right)}$		4	$\left(\frac{2}{1-\xi}\right)\left(\frac{1+\eta}{1-\eta}\right)$

For the field variable mapping functions of both elements, however, Lagrangian functions are used (Equation 6).

$$\{u\} = \left(L_j\right)\left(L_k\right)\{d_i\} \tag{19}$$

The eight-node or five-node infinite elements can be coupled with eight-node, quadrilateral, finite elements. Gauss-Legendre numerical integration is used to form the element stiffness matrix; [K] is employed for the solution of the case studies.

QUANTITATIVE COMPARISONS

In order to benchmark the predictive capabilities of infinite elements, closed form solutions of the Boussinesq problem (Poulos and Davis 1974) are compared with finite element modeling of a soil body (semi-infinite medium) with and without infinite elements. Axi-symmetric analyses are performed due to cylindrical symmetry or axi-symmetry. The body is formed by the revolution of meshed parts creating the Finite Element Model on a section plane on one side of the rotational axis and loads and constraints acting on the part are only radial and axial, with no tangential component (Logan 2002). A slice of semi-infinite medium, with one radian central angle reduces the size of the finite element model, thereby decreasing the solution time. Two different cases with distinct modeling scenarios are considered.

Example 1: Circular Uniform Distributed Loading on Semi-infinite Medium

A circular tank on the ground is studied, as is frequently encountered in geotechnical engineering. For this, a closed form solution of the problem is available (Jumikis 1969). The tank is $2a=10\ m$ in diameter. The applied pressure on the ground when the tank is full is 40 kPa. Figure 7 shows the schematic diagram of the problem including the foundation region considered in the analysis. The soil is assumed to be linear and isotropic with a Young's Modulus; $E = 4\ 000\ kPa$ and a Poisson's ratio; $v = 0.40$. Since the problem is cylindrically symmetrical about the vertical center-line of the tank, the required finite element grid extends out from the tank center-line for axi-symmetric analyses.

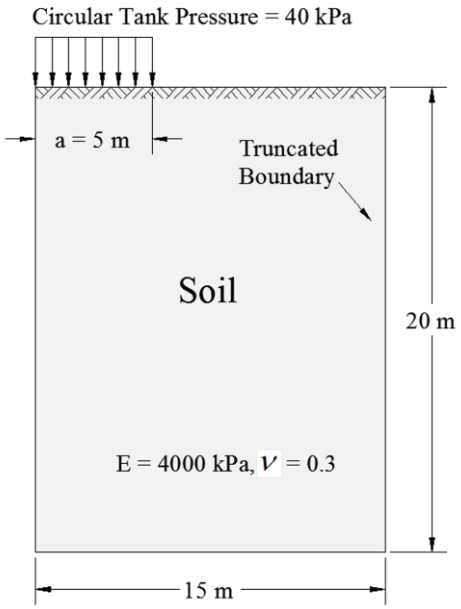

Figure 7. Circular tank on the ground

In the finite element modeling of the problem, a 3 x 4 axi-symmetric coarse mesh and 6 x 8 axi-symmetric fine mesh, consisting of eight-node high order quadrilateral elements are generated (Figure 8). The truncation of the domain of analysis is usual in such a case. The mesh configurations used in this paper differs from other studies (Abdel-Fattah et al. 2000) in that all elements have an aspect ratio of 1.The numerical analyses are conducted using the computer package program *GeoStudio SIGMA/W* (GeoStudio 2004a and 2004b). Along the axis of symmetry, coinciding with the vertical truncation boundary, a boundary condition of zero horizontal displacement is imposed. The horizontal truncation boundary at the bottom edge has zero vertical displacements. Movable hinge supports are assumed all along the three, mutually, perpendicular, boundary lines.

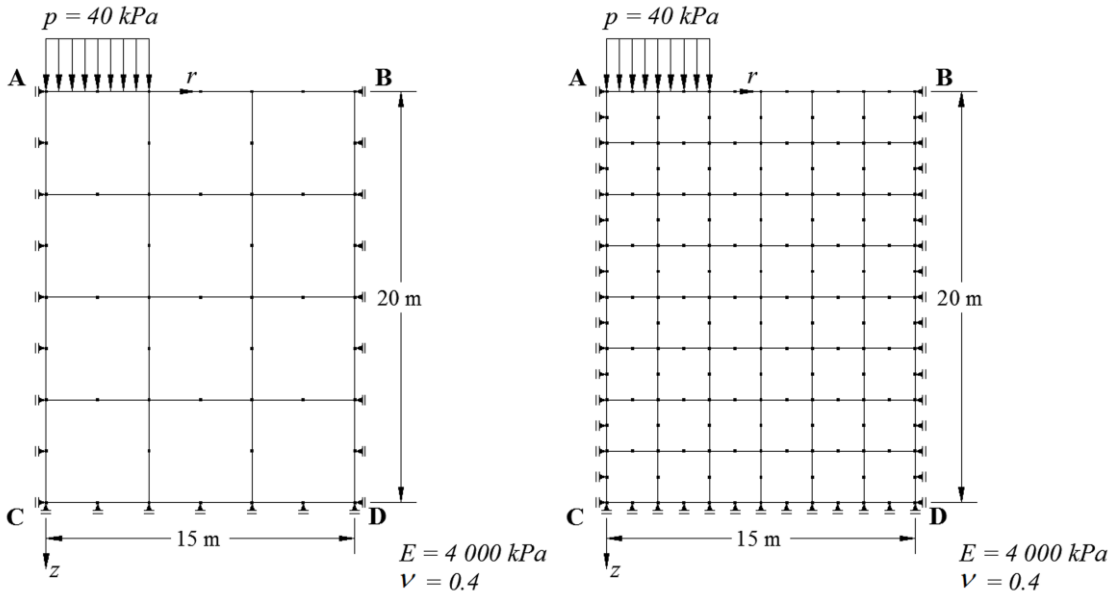

Figure 8. Coarse and fine meshes of an axi-symmetric body with rigid truncation boundaries

For the purpose of introducing infinite elements at the truncation lines CD and BD, third and fourth models are generated by attaching a corridor of eight-node, high-order, quadrilateral infinite elements all along the two truncation boundaries (CD and BD). Thus, the 3 x 4 coarse mesh and the 6 x 8 fine mesh were created as shown in Figure 9. The infinite elements are indicated by an arrowhead specifying their direction to infinity.

The vertical stresses and the vertical displacements along the vertical, central axis through the center of the circular area are calculated by three distinct methods:

- Two finite element models with truncated boundaries – one with a 3 x 4 coarse mesh and one with a 6 x 8 fine mesh;
- The same two abovementioned meshes with infinite elements along the bottom and right-hand side truncation boundaries using GeoStudio SIGMA/W package program (GeoStudio 2004a and 2004b);
- The exact formulation (Poulos and Davis, 1974);

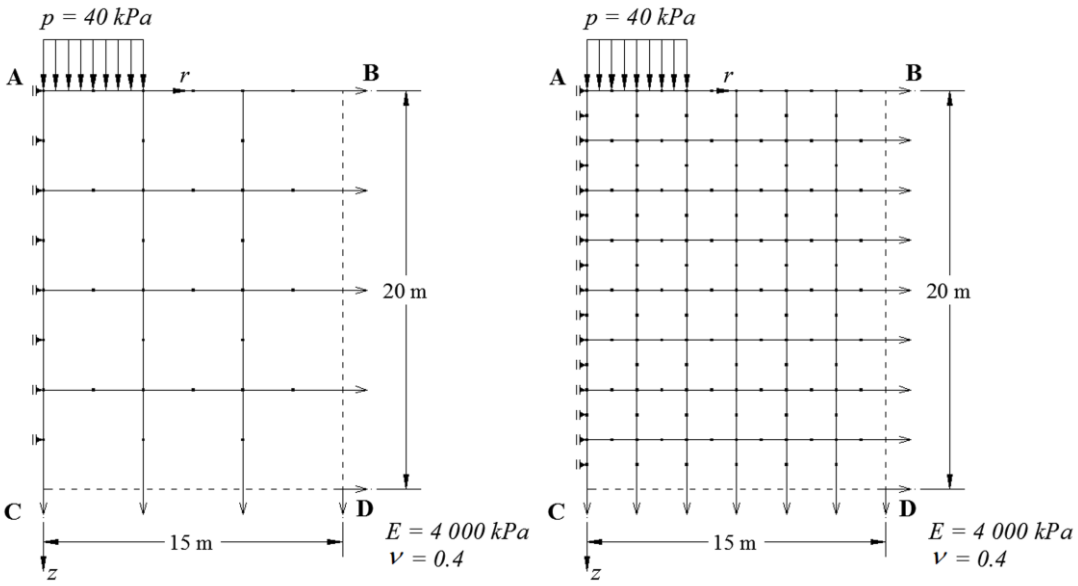

Figure 9. Coarse and fine meshes of an axi-symmetric body with infinite elements along the truncation boundaries

According to the analytical solution, the vertical stress and the vertical displacement along the vertical, central axis through the center of the circular area are given in Equations (20) and (21), respectively.

$$\sigma_z = p\left[1-\left(\frac{1}{1+(a/z)^2}\right)^{3/2}\right] \tag{20}$$

$$w = \frac{2pa\left(1-\nu^2\right)}{E}\left(\sqrt{1+(z/a)^2}-z/a\right)\left[1+\frac{z/a}{2(1-\nu)\sqrt{1+(z/a)^2}}\right] \tag{21}$$

where p is the uniformly distributed loading over the circular bearing area, a is the radius of the circular bearing area, z is the depth, ν is the Poisson's ratio of the medium, and E is the Young's Modulus of the medium. The vertical stresses and displacements calculated by these three methods, along the vertical, central axis through the center of the circular area are illustrated graphically in Figures 10 and 11, respectively.

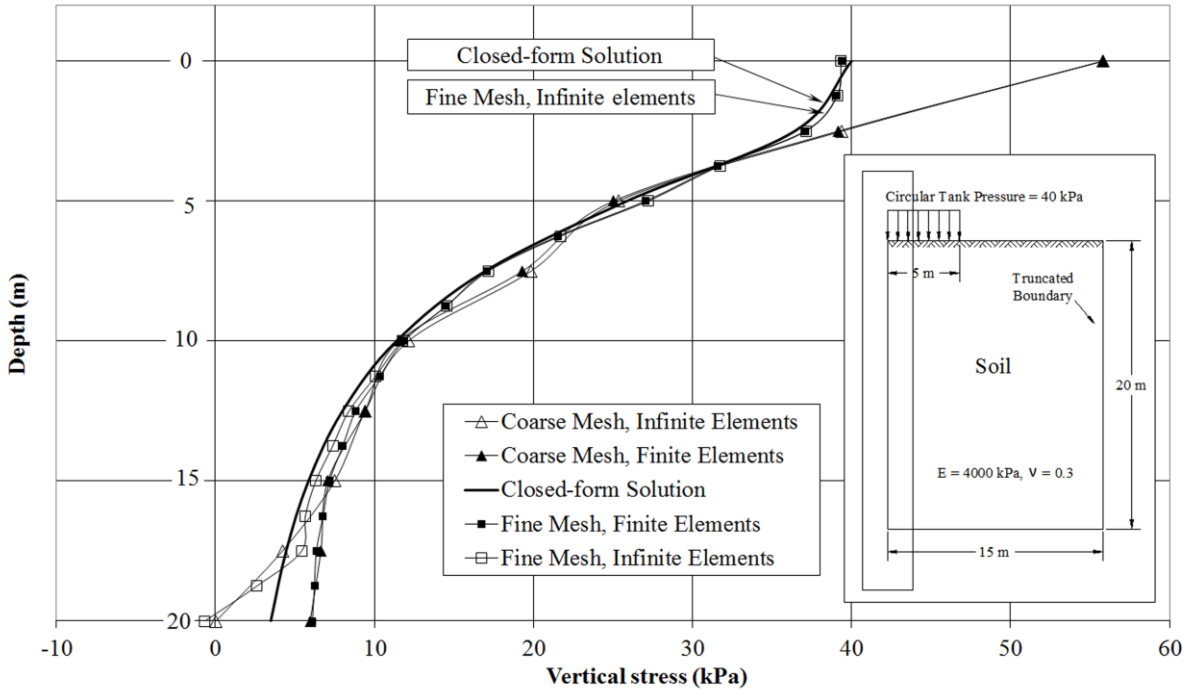

Figure 10. Vertical stresses along the vertical central axis

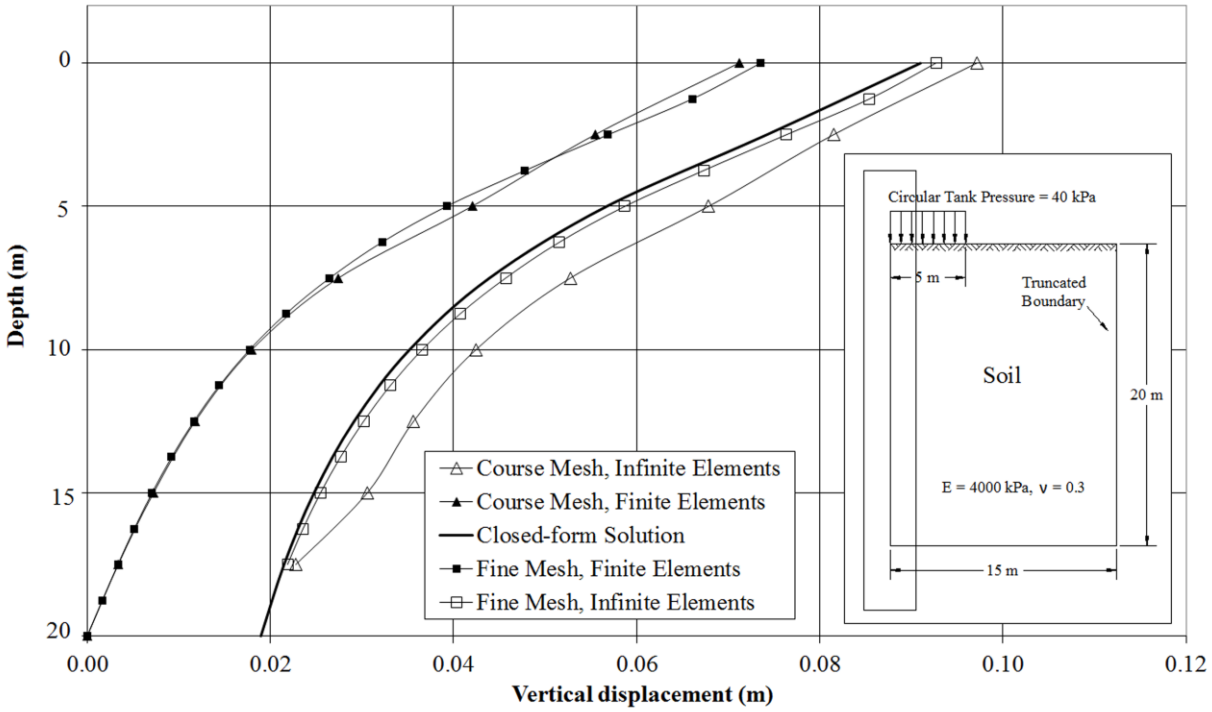

Figure 11. Vertical displacements along the vertical central axis

Evaluation of the Results of the Circular, Uniform, Distributed Loading

Even for a relatively coarse mesh, having only 12 elements (3 x 4) (Figure 9), the improvement of results over a similar analysis with infinite elements is evident. This is most clear in the displacement values along the vertical central axis (Figure 11). When a finer mesh (6 x 8) is employed, almost no changes occur in the displacements. However, the same mesh with infinite elements along the bottom and right-hand side truncation boundaries gives exact results.

Other studies also made various attempts to solve the similar unbounded domain problems by employing different analysis parameters. For example, Koh and Lee (1998) analyzed the settlement variation at a point 2m deep below the circular footing by incrementally expanding the size of the analysis domain. They needed to increase the side lengths of the rectangular analysis domain up to 50 times to overcome an error of approximately 32% and to obtain a numerical solution nearly identical to the analytical solution. Here, however, the vertical deflection at the surface of a semi-infinite medium under a circular uniform loading is 91.0mm by the exact theory. The errors for the 3 x 4 coarse mesh and 6 x 8 fine mesh sizes are 21.7% and 19.2%, respectively. When infinite elements with a coarse, 3 x 4 mesh size are used, the error is reduced to 6.7%. The performance of high order elements with aspect ratios of 1 contributed to the accuracy.

Because stresses are secondary dependent variables; when infinite elements are used, the improvement in stress results is not as significant as displacement results. However, improved convergence with mesh refinement is observed (Figure 10). The stress variation obtained from the fine meshes with infinite elements closely reflects the exact solution.

Example 2: A Point Load on a Semi-infinite Medium and Sensitivity Analysis of Finite Element Modeling

As a second example, a singular point load acting on a soil body is considered. The effect of the enlargement of the domain of analysis (frequently used in finite element modeling of soils) and the effect of springs used all along the truncation boundaries of unbounded domain problems are investigated by performing axi-symmetric analyses (Figure 12).

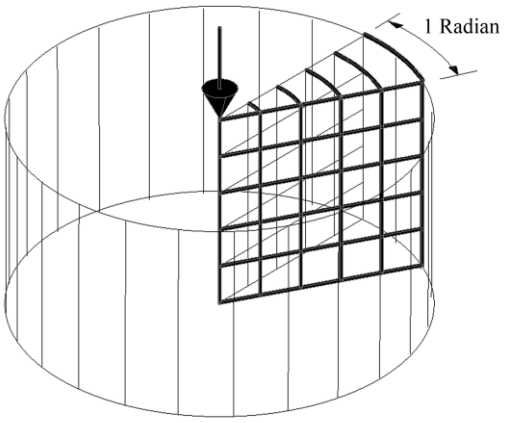

Figure 12. Singular load on an axi-symmetric, semi-infinite medium and a slice taken from it for analysis

The material is assumed to be linear and isotropic with a Young's Modulus E = 2,000 MPa and a Poisson's ratio ν = 0.40. The point load acting vertically at the center of a 3-D elastic half space is P = 3,000 kN. The computer package program GeoStudio SIGMA/W is used in the analyses. The vertical displacements, beneath the point load, are calculated with five distinct finite element models using the same size finite elements and the exact formulation as follows:

- Finite element modeling with a 5 x 5 mesh (3m×3m), with truncated boundaries (Figure 13a).
- Finite element modeling with a 5 x 5 mesh, using springs along the truncated boundaries (Figure 13b),
- Finite element modeling with a 5 x 5 mesh with infinite elements attached to the bottom and right-hand side boundaries (13c),
- Finite element modeling with a 25 x 25 mesh (15m×15m), with truncated boundaries (Figure 13d)
- Finite element modeling with a 50 x 50 mesh (30m×30m), with truncated boundaries (Figure 13e)
- The exact formulations by Boussinesq (as reported by Jumikis 1969).

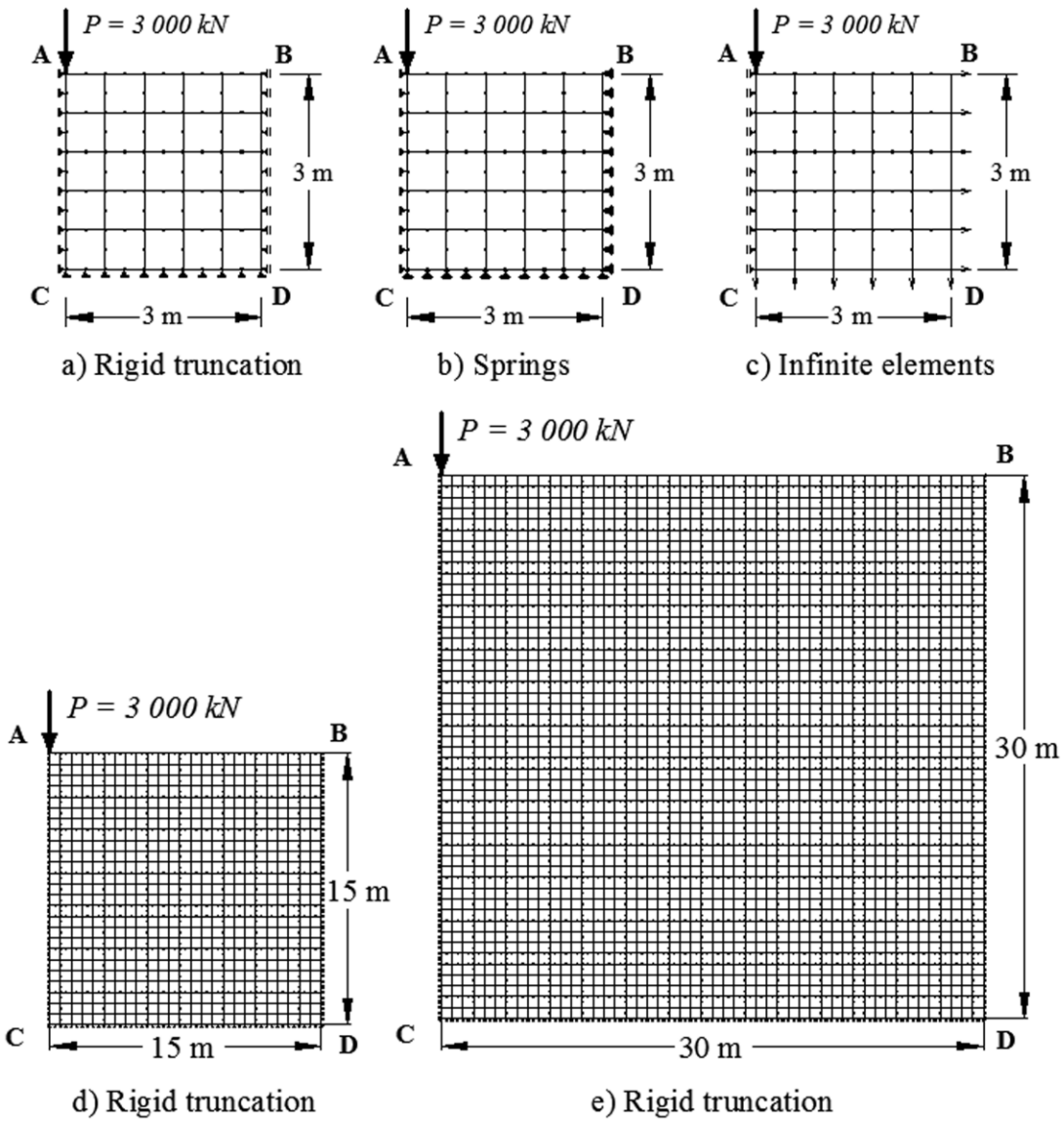

Figure 13. Meshes used in finite element modeling of axi-symmetric body (5 x 5 for a, b, c; 25 x 25 for d; and 50 x 50 for e)

Introduction and Determination of Spring Properties

The use of infinite elements for unbounded domain modeling is first compared to the use of springs. Therefore, for a more realistic behavior of soil along the truncation boundaries, springs are defined at boundary nodes. Each spring coefficient is calculated as the product of the coefficient of the subgrade reaction of the soil, k_s, and the relevant tributary area of each node since k_s is defined as the bearing pressure to produce unit displacement (Coduto 2001). Based

on the work by Tezcan and Özdemir (2011), the empirical relationship in Equation 22 can be derived to be expressed as k_s .

$$k_s = \sqrt{\frac{8 E g \gamma}{(1+\nu)}} \tag{22}$$

where, E is the modulus of elasticity (2,000MN/m^2); g is the gravity (9.81m/s^2); γ is the unit weight (25kN/m^3) and ν (0.40) is the Poisson ratio of the soil. Using the prescribed units, k_s is estimated as 52,942kN/m^3.

Evaluation of the Results of the Boussinesq Problem

The vertical displacements and associated errors with respect to the closed-form solution obtained by employing a 5 x 5 mesh with and without infinite elements along the r = 0.6m line and the z = 1.2m horizontal line are illustrated in Figures 14 and 15, respectively. Very good agreement exists with the exact solutions when quadratic infinite elements are used. Displacement error percentages also confirm this.

Even with infinite elements, slightly higher displacement error percentages near the point load along the vertical line at r = 0.6m are observed in Figure 14. This is because the errors increase due to the singularity effect of the point load, which was observed previously by El-Esnawy et al (1995). They solved the same problem using 48 eight-node, tri-linear, finite elements coupled with 28 decay function infinite elements and made a comparison with a model, meshed using only finite elements. They reported high performance of infinite elements. However, their models were not equivalent to each other because the model with only finite elements included 120, eight-node, tri-linear finite elements (being comprised of much larger number of elements); the equivalence of the models being compared is crucial to quantify accuracies.

In the evaluation herein with an equivalent number of elements, accuracies improve remarkably with larger depths when infinite elements are used herein. Errors remain within 12%, unlike when using pure finite elements. Figure 15 shows that the displacement values z = 1.2m horizontal line obtained when infinite elements are employed are almost identical to the closed form solutions. Errors stay within 3.5%, whereas the pure finite element solutions are relatively far from the exact results.

Note, however, that due to stress concentrations in the vicinity of the point load, the accuracy of the numerical solution even with infinite elements may differ slightly from the exact solution. In general, the regular finite element solutions underestimate the displacements. The situation is greatly improved by the introduction of the infinite elements, with only minimal additional computational effort. For instance, the error percentage for the vertical deflection at 1.5m depth below the point load is 45% when a coarse 5 x 5 mesh is used (Figure 16). The error is only reduced to 3% when a 50 x 50 fine mesh is used, which is 10 times greater in field size and 100 times greater number of finite elements. When infinite elements are used however, with only a 5 x 5 mesh, the error is a mere 1%.

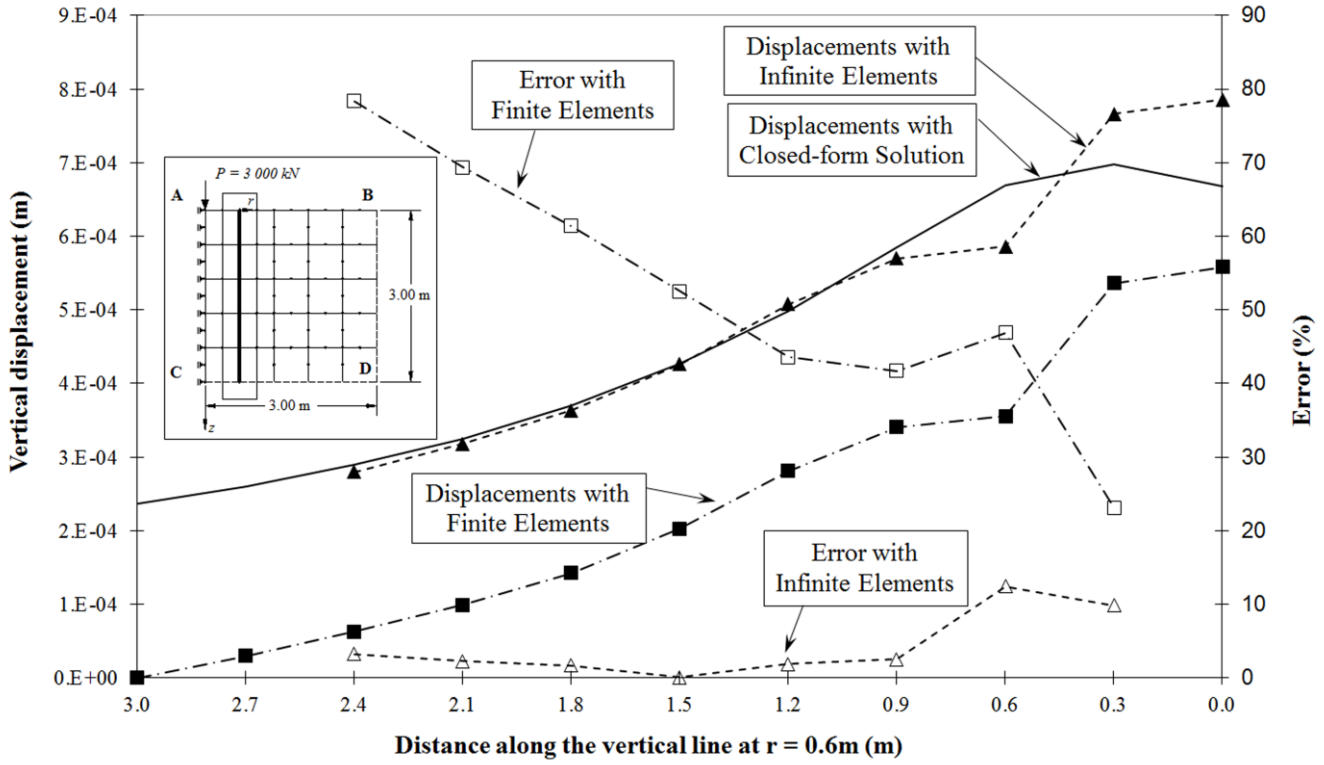

Figure 14. Displacements and associated errors along the vertical line at r = 0.6 m

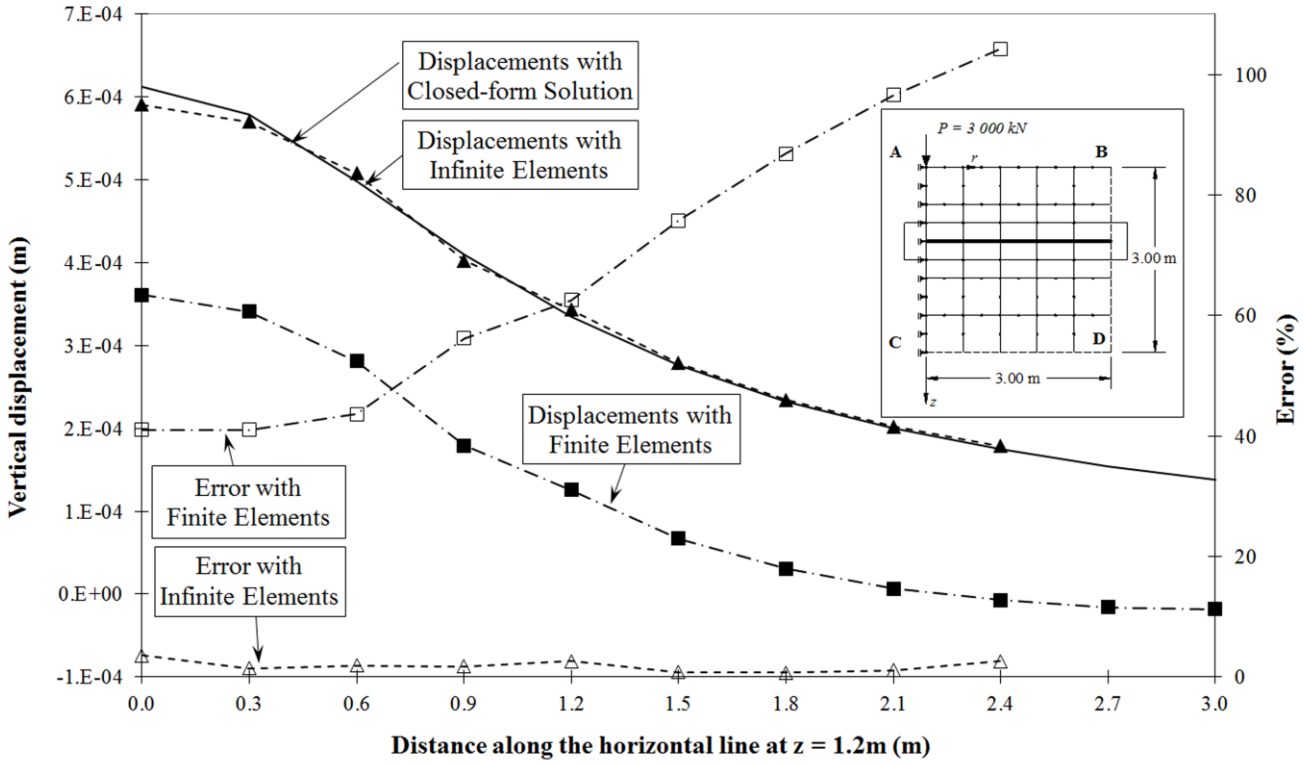

Figure 15. Displacements and associated errors along the horizontal line at z = 1.2 m

The vertical displacements along the vertical axis at r = 0m (calculated by the six methods described above) are illustrated in Figure 16. The effect of the enlargement of the analysis domain was investigated by increasing the side length of the analysis domain from 3m to 15m and then to 30m. With the increase in the size of the analysis domain, the results in the area of interest converged to the closed-form solutions. However, while the accuracy of the results improved, 2,500 finite elements were required, instead of only 25. Restricting the number of elements to 25 and using springs at boundary nodes generated better results than those of the coarse or fine meshes with truncated boundaries. However the coarse mesh of 5 x 5 with infinite elements along the truncated boundaries gives consistently more accurate results, when compared with equivalently sized meshes (5 x 5, 25 x 25, and 50 x 50) with truncated boundaries with respect to the exact solution. Table 2 presents error percentages of considered solution methods along the core of the analysis domain and proves the superiority of infinite elements, in such cases.

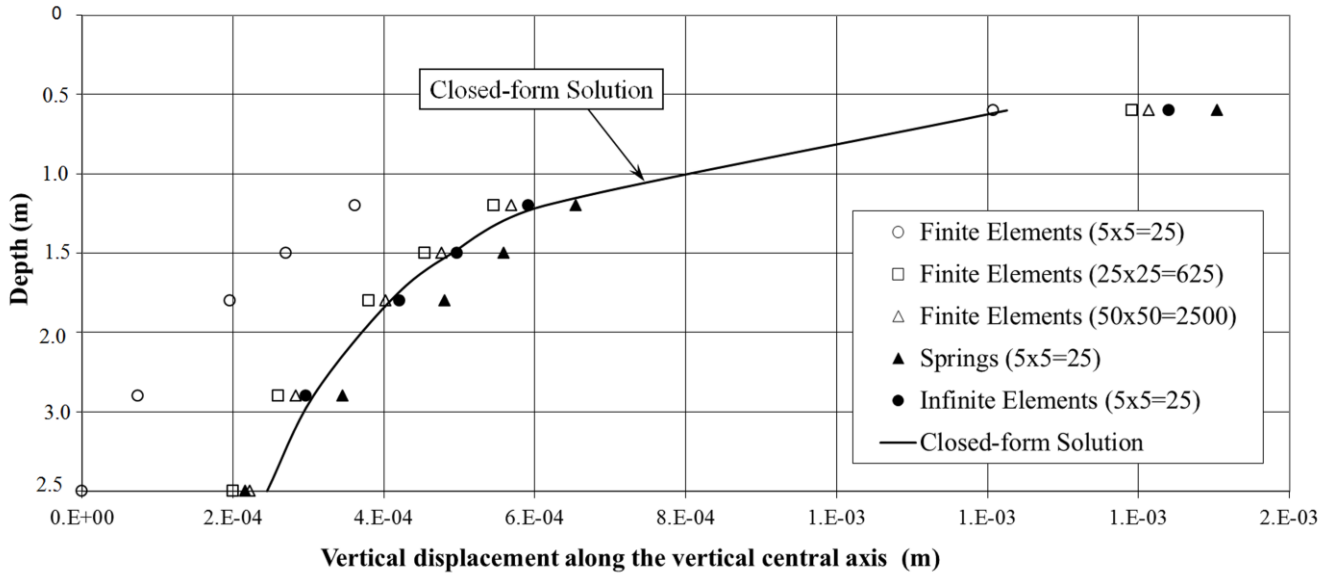

Figure 16. Vertical displacements along the vertical central axis (where the point load acts)

Table 2. Displacement errors of solution methods

Depth under point load (m)	Displacement Errors (%)				
	5 x 5 fixed boundary	25 x 25 fixed boundary	50 x 50 fixed boundary	5 x 5 with springs	5 x 5 with infinite elements
0.6	76	15	7	13	3
1.2	52	7	1	18	3
1.5	45	7	3	14	1
1.8	41	11	7	7	4

SUMMARY AND CONCLUSIONS

This paper provides the accurate quantification of the advantages of the use of infinite elements versus the introduction of a truncated boundary or other approximate means. This is done through the introduction and presentation of a comprehensive set of coordinate and field variable mapping functions of 1-D and 2-D infinite elements, not previously available. The approach is benchmarked against two problems with known solutions. The results were as follows:

1) The formulation of the stiffness matrices and all other properties of an infinite element were shown to be similar to that used for the conventional finite elements. Specifically, through the appropriate selection of shape functions for both coordinates and field variables, the derivation of matrix properties becomes a straightforward operation.

2) The adaptation of an infinite element into a standard finite element package program introduced no special difficulties, because the infinite elements retain the narrow bandwidth nature of the master stiffness matrix, while requiring less memory.

3) The infinite elements systematically provided a high degree of accuracy in unbounded continuum problems, even with relatively coarse mesh sizes.

4) The introduction of infinite elements was a more computationally efficient means to increase accuracy than the employment of a finer mesh with a higher number of finite elements. To achieve the same results with finite elements required an excessive introduction of elements.

5) Infinite elements generated superior results compared to the placement of equivalent springs along truncated boundaries.

ACKNOWLEDGMENTS

The authors greatly acknowledge the support and feedback of Prof. Dr. Yalçın Aköz throughout this study.

REFERENCES

Abdel-Fattah, T. T., Hodhod, H. A. and Akl, A. Y. (2000). "A novel formulation of infinite elements for static analysis." *Comp. Struc.,* 77(4), 371-379.

Anderson, D. L. and Ungless, R. L. (1977). "Infinite finite elements", *Int. Symp. on Innovative Num. Anal. Appl. Eng. Sci.*, Versaille, France.

Beer, G. and Meek, J. L. (1981). "Infinite domain elements." *Int'l J. Num. Meth. Eng*., 17(1), 43-52.

Bettess, P. (1977). "Infinite elements." *Int'l J. Num. Meth. Eng*., 11(1), 53-64.

Bettess, P. (1980). "More on infinite elements." *Int'l J. Num. Meth. Eng*., 15(11), 1613-1626.

Bettess, P. (1992). *Infinite elements*, Penshaw Press, Sunderland, U.K.

Bettess, P. and Zienkiewicz, O. C. (1977). "Diffraction and refraction of surface waves using finite and infinite elements." *Int'l J. Num. Meth. Eng*., 11(8), 1271-1290.

Coduto, P. D. (2001). *Foundation design: principles and practices*, Prentice-Hall, New Jersey.

Damjanlć, F. and Owen D. R. J. (1984). "Mapped infinite elements in transient thermal analysis." *Comp. & Struct.*, 19(4), 673-687.

Deeks, A. J. and Randolph, M. F. (1994). "Axisymmetric time-domain transmitting boundaries." *J. Eng. Mechanics*, 120(1), 25-42.

El-Esnawy, N. A., Akl, A. Y. and Bazaraa, A. S. (1995). "A new parametric infinite domain element." *Finite Elements in Analysis and Design*, 19(1-2), 103-114.

GeoStudio (2004a). Stress and Deformation Modeling with SIGMA/W, *(Version 6.02) [Software],* GEO-SLOPE International Ltd, Calgary, Alberta, Canada. Available from http://www.geo-slope.com/products/sigmaw.aspx

GeoStudio (2004b). Analysis Reference, Stress and Deformation Modeling with SIGMA/W, GEO-SLOPE International Ltd, Calgary, Alberta, Canada, 2004.

Jumikis, A. R. (1969). *Theoretical soil mechanics: with practical applications to soil mechanics and foundation engineering*, Van Nostrand Reinhold Co., New York.

Katsikadelis, J. T. (2002). *Boundary elements: theory and applications*, 1st Edition, Elsevier Science. Oxford, UK.

Kausel, E. (1988). "Local transmitting boundaries." *J. Eng. Mech.*, 114(6), 1011-1027.

Kazakov, K. S. (2010). "Elastodynamic infinite elements with united shape functions for soil–structure interaction." *Finite Elements in Analysis and Design*, 46(10), 936-942.

Khalili, N., Valliappan, S., Yazdi, J.T., Yazdchi, M. (1997). "1D infinite element for dynamic problems in saturated porous media." *Comm. Num. Meth. Eng.*, 13(9) 727-738.

Koh, K. H. and Lee, S. R. (1998). "P-version static infinite element for representing $1/r^n$ type decay problems in unbounded media." *Comp. Geotech.*, 22(1), 73-89.

Logan, D. L. (2002). *First course in the finite element method*, Thomson Learning, Pacific Grove, California, USA.

Medina, F. (1980). "Modelling of soil-structure interaction by finite and infinite elements" Ph.D. Thesis, University of California, Berkeley.

Medina, F. (1981). "An axisymmetric infinite element", *Int'l J. Num. Methods Eng.*, 17, 1177-1185.

Poulos, H. G. and Davis, E. H. (1974). *Elastic solutions for soil and rock mechanics*, John Wiley & Sons, Inc, NY.

Simoni, L. and Schrefler, B. A. (1987). "Mapped infinite elements in soil consolidation", *Int'l J. Num. Methods Eng.*, 24, 513-527.

Tezcan S. S. and Ozdemir Z. (2011). "A refined formula for the allowable soil pressure using shear wave velocities." *The Open Civil Eng. J.*, 5, 1-8.

Ungless, R. F., (1973). "Infinite finite element." M.S. Thesis, University of British Columbia, BC Canada.

Xia, K., and Zhang, Z. (2006). "Three-dimensional finite/infinite elements analysis of fluid flow in porous media." *Applied Mathematical Modelling*, 30(9), 904-919.

Yang, Y. B., Hung, H. H., and Chang, D. W. (2003). "Train-induced wave propagation in layered soils using finite/infinite element simulation." *Soil Dyn. Earthquake Eng.*, 23(4), 263-278.

Zhao, C. and Valliappan, S. (1993). "Transient infinite elements for seepage problems in infinite media", *Int'l J. Num. Anal. Meth. Geomechanics*, 17(5), 323-341.

Zienkiewicz, O. C. and Bettess, P. (1975). "Infinite elements in the study of fluid structure interaction problems." *Proc. 2nd Int. Symp.On Comp. Methods Appl. Sci.*, Versailles, France. Also published in "Lecture Notes in Physics."(1976) Eds. J. Ehlers et al., Springer-Verlag, Berlin.

Zienkiewicz, O. C., Emson, C. and Bettess, P. (1983). "A novel boundary infinite element." *Int. J. Num. Meth. Eng.*, 19(3), 393-404.